

# Inductive Superconducting Quantum Interference Proximity Transistor: The L-SQUIPT

Federico Paolucci<sup>1,\*</sup>, Paolo Solinas,<sup>2,3</sup> and Francesco Giazotto<sup>1,†</sup>

<sup>1</sup>NEST, Istituto Nanoscienze-CNR and Scuola Normale Superiore, Pisa I-56127, Italy

<sup>2</sup>Dipartimento di Fisica, Università di Genova, via Dodecaneso 33, Genova I-16146, Italy

<sup>3</sup>INFN - Sezione di Genova, via Dodecaneso 33, Genova I-16146, Italy



(Received 8 March 2022; revised 3 August 2022; accepted 12 September 2022; published 15 November 2022)

The design for an *inductive* superconducting quantum interference proximity transistor with enhanced performance, the L-SQUIPT, is presented and analyzed. The interferometer is based on a double-loop structure, where each ring comprises a superconductor–normal-metal–superconductor mesoscopic Josephson weak link and the readout electrode is implemented in the form of a superconducting tunnel probe. Our design allows us to both improve the coupling of the transistor to the external magnetic field and increase the characteristic magnetic flux transfer functions, thereby leading to an improved ultrasensitive quantum limited magnetometer. The L-SQUIPT behavior is analyzed in both the *dissipative* and the *dissipationless* Josephson-like operation modes, in the latter case by exploiting both an inductive and a dispersive readout scheme. The improved performance makes the L-SQUIPT promising for magnetic flux detection as well as for specific applications in quantum technology, where a responsive dispersive magnetometry at millikelvin temperatures is required.

DOI: [10.1103/PhysRevApplied.18.054042](https://doi.org/10.1103/PhysRevApplied.18.054042)

## I. INTRODUCTION

The superconducting quantum interference device (SQUID) is currently one of the most used magnetometers on the market [1]. A SQUID consists of a superconducting ring interrupted by two Josephson junctions; thus, its critical current strongly depends on the magnetic flux ( $\Phi$ ) piercing the loop [2]. To achieve sizable magnetic field sensitivities, SQUIDs typically employ large pickup loops, yielding a best intrinsic flux noise of the order of about  $1 \mu\Phi_0/\sqrt{\text{Hz}}$  [1], where  $\Phi_0 = 2.067 \times 10^{-15}$  Wb is the magnetic flux quantum. Differently, scanning nanoscale SQUIDs showed a flux noise as low as  $50 \text{n}\Phi_0/\sqrt{\text{Hz}}$  thanks to low inductance loops and the vicinity to the magnetic moment source [3], but a lower magnetic field sensitivity.

Last decade witnessed the advent of another sensitive magnetometer: the superconducting quantum interference proximity transistor (SQUIPT) [4]. It is realized in the form of a superconducting ring embodying a normal metal (SNS) [5–10] or superconducting ( $SS_1S$ ) [11–13] nanowire Josephson junction. Thanks to the superconducting proximity effect [14,15], a phase-dependent miniband ( $E_g$ ) appears in the density of states (DOS) of the nanowire [16]. The latter is modulated by the superconducting phase

difference built across the nanowire generated by the magnetic flux piercing the superconducting ring. Indeed, the current versus voltage characteristics of a tunnel probe (normal metal or superconductor) directly coupled to the proximitized Josephson junction is strongly  $\Phi$  dependent. In the SQUIPT, the readout operation is typically performed by recording the current (voltage) as a function of  $\Phi$ , while the tunnel probe is voltage (current) biased. Thus, the SQUIPT operates as a transducer of the magnetic field into a current (voltage).

The best experimental flux sensitivity achieved so far in a SNS SQUIPT reaches  $500 \text{n}\Phi_0/\sqrt{\text{Hz}}$  at  $240 \text{ mK}$  [6], while it reaches about  $260 \text{n}\Phi_0/\sqrt{\text{Hz}}$  at  $1 \text{ K}$  for a  $SS_1S$  device [12]. These values are a few orders of magnitude larger than the limiting theoretical flux noise of about  $1 \text{n}\Phi_0/\sqrt{\text{Hz}}$  [17], because the SQUIPT magnetometer shows different weaknesses and structural drawbacks. In particular, the SQUIPT suffers from low coupling between the external magnetic field and the superconducting loop. Indeed, a conventional device needs a small loop in order to have a negligibly small ring inductance compared to the junction Josephson inductance. Only under this assumption full phase bias does occur across the proximitized junction, thereby allowing an efficient flux-induced modulation of the DOS of the weak link. Furthermore, the phase biasing of the junction is efficient only for an almost-sinusoidal current-phase relation (CPR), since in such a case the Josephson inductance of the weak link at  $\pi$  is

\*federico.paolucci@pi.infn.it

†francesco.giazotto@sns.it

always finite [18,19]. By contrast, a sizable flux sensitivity of the SQUIPT would be achieved by exploiting nanowire junctions in the *short* limit ( $\Delta_0 \leq \hbar D/L^2$ , where  $\Delta_0$  is the zero-temperature gap of the superconductor,  $\hbar$  is the reduced Planck constant, and  $D$  and  $L$  are the diffusion constant and the physical length of the nanowire, respectively) [11,20,21], since in this regime the CPR is a nonsinusoidal function of the phase ( $\varphi$ ) [18,19]. Yet, in the *short* limit and for low temperatures, the Josephson inductance is effectively vanishing at  $\varphi \rightarrow \pi$ , thus preventing the full phase biasing of the junction. Therefore, a conventional SQUIPT needs to be operated at higher temperatures, where the Josephson inductance is finite, but the sensitivity can be sizeably reduced. Furthermore, fully superconducting SQUIPTs in the *long-junction* limit present CPRs hysteretic with direction of the phase biasing (external magnetic flux) [11,22], thus hampering their application as magnetometers.

Here, we propose an inductive superconducting quantum interference proximity transistor (i.e., the L-SQUIPT) that solves the above-described intrinsic limitations typical of conventional SQUIPT magnetometers. To this end, the L-SQUIPT takes advantage of a double-loop geometry to efficiently bias the second SNS Josephson junction assumed to be in the *short* limit. Furthermore, by employing a superconducting tunnel probe, the L-SQUIPT readout operation can be realized either through a dissipative (quasiparticle tunneling) or via dissipationless (Josephson supercurrent) measurements depending on the requirements of the specific application. The L-SQUIPT is predicted to show a best quantum limited noise as low as a few  $n\Phi_0/\sqrt{\text{Hz}}$ , thus improving the sensitivity achievable with conventional SQUIPT and SQUID magnetometers. This makes the L-SQUIPT potentially relevant for magnetic field detection as well as for other applications in the field of quantum technologies [23].

This paper is organized as follows: Sec. II presents the structure of the L-SQUIPT and the basic equations describing the SNS Josephson junctions embedded in the superconducting rings; Sec. III shows the phase biasing of the output SNS Josephson junction by the external magnetic flux; Sec. IV describes the dissipative readout of the L-SQUIPT in both voltage and current bias operations; Sec. V presents the dissipationless readout realized by means of inductive and dispersive measurement schemes; and Sec. VI resumes the concluding remarks.

## II. STRUCTURE

The L-SQUIPT is composed of two superconducting loops, each of them interrupted by a normal-metal weak link forming a SNS Josephson junction, as shown in Fig. 1(a). The first loop (of inductance  $L_1$ ) converts the external magnetic flux ( $\Phi_1$ ) into a superconducting phase drop ( $\varphi_1$ ) across the Josephson junction ( $J_1$ , orange), i.e., it operates

a flux-to-phase conversion ( $\Phi_1 \rightarrow \varphi_1$ ). In order to have an efficient coupling to the external magnetic field, the first superconducting loop, in principle, needs to be sufficiently large. To optimize the  $\Phi_1 \rightarrow \varphi_1$  conversion, we suppose that the CPR of  $J_1$  is sinusoidal (diffusive *long-junction* limit), that is [18]

$$I_{J1}(T) = I_{C1}(T) \sin(\varphi_1), \quad (1)$$

where  $I_{C1}(T)$  is the temperature-dependent critical current of the  $J_1$  junction and  $T$  is the temperature. A simplified equation for the critical current of  $J_1$  can be found in the high-temperature regime, that is, for  $k_B T > 5E_{\text{Th}}$ , where  $k_B$  is the Boltzmann constant and  $E_{\text{Th}} = \hbar D/L^2$  is the Thouless energy. In this limit it reads

$$I_{C1}(T) = \frac{64\pi k_B T}{eR_1} \sum_{n=0}^{\infty} \times \frac{(\sqrt{2\omega_n/E_{\text{Th}}})\Delta^2(T) \exp[-\sqrt{2\omega_n/E_{\text{Th}}}] }{[\omega_n + \Omega_n + \sqrt{2(\Omega_n^2 + \omega_n\Omega_n)}]^2}, \quad (2)$$

where  $e$  is the electron charge,  $R_1$  is the normal-state resistance of the junction,  $\Delta(T)$  is the temperature-dependent superconducting energy gap of the ring,  $\omega_n(T) = (2n+1)\pi k_B T$  is the Matsubara frequency, and  $\Omega_n(T) = \sqrt{\Delta^2(T) + \omega_n^2(T)}$ .

We suppose that the second loop (of inductance  $L_2$ ) is fully screened from the external magnetic field (thus  $\Phi_2 = 0$ ), for instance through a superconducting plate [gray rectangle in Fig. 1(a)] electrically separated from the device by means of an insulating layer, and operates as a phase-to-phase ( $\varphi_1 \rightarrow \varphi_2$ ) transformer. Inductance  $L_2$  needs to be sufficiently small in order to limit the phase drop along the smaller superconducting ring and, thus, to maximize the efficiency of the  $\varphi_1 \rightarrow \varphi_2$  transformation. Junction  $J_2$  (red) is supposed to be in the *short* limit, thus obeying the diffusive Kulik-Omel'yanchuk (KO) model [24]. Therefore, the temperature-dependent CPR of a  $J_2$  takes the form

$$I_{J2}(\varphi_2, T) = \frac{\pi \Delta(T)}{eR_2} \Xi(\varphi_2, T), \quad (3)$$

where  $R_2$  is the normal-state resistance of  $J_2$ . The phase dependence in the diffusive KO model takes the form [24]

$$\Xi(\varphi_2, T) = \cos\left(\frac{\varphi_2}{2}\right) \times \int_{\Delta(T) \cos(\varphi_2/2)}^{\Delta(T)} \frac{\tanh(\varepsilon/k_B T)}{\sqrt{\varepsilon^2 - \Delta^2(T) \cos^2(\varphi_2/2)}} d\varepsilon. \quad (4)$$

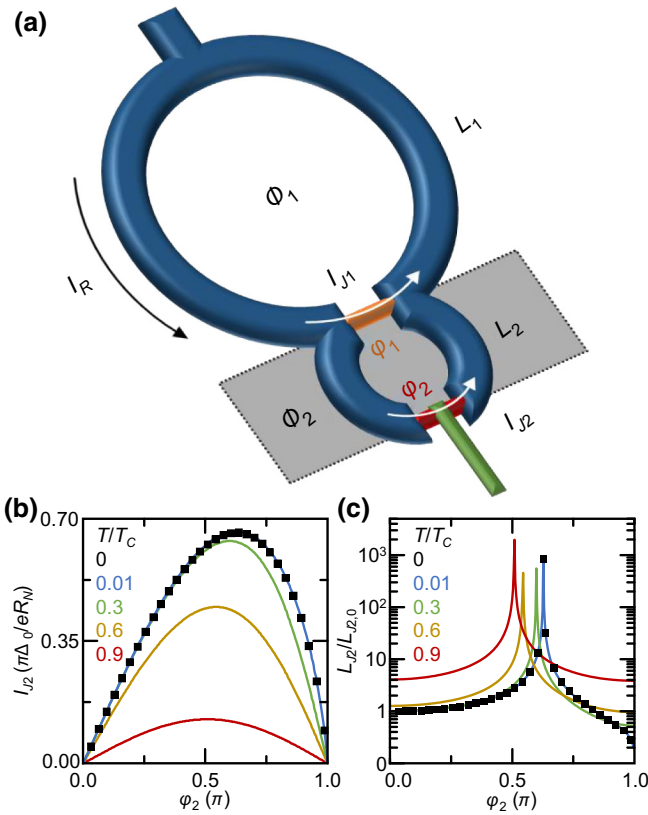


FIG. 1. (a) Scheme of the L-SQUIPT. The device is composed of two superconducting loops of inductances  $L_1$  and  $L_2$  interrupted by the two SNS Josephson junctions ( $J_1$  and  $J_2$ ) of Josephson switching currents  $I_{J1}$  and  $I_{J2}$ , respectively. The second ring is supposed to be screened against the external magnetic field ( $\Phi_2 = 0$ ). Therefore, the phase drop across the two junctions is equal ( $\varphi_1 = \varphi_2$ ). (b) Diffusive Kulik-Omel'yanchuk current-to-phase relation (KO CPR) of  $J_2$  calculated in the short-junction limit for different temperatures. (c) Normalized Josephson kinetic inductance ( $L_{J2}/L_{J2,0}$ ) calculated from the diffusive KO CPR. Here  $L_{J2,0}$  is the zero-temperature and zero-phase kinetic inductance of  $J_2$ .

In the zero-temperature limit ( $T = 0$ ), the KO CPR can be simplified as [24]

$$I_{J2}(\varphi_2, T = 0) = \frac{\pi \Delta_0}{eR_2} \cos\left(\frac{\varphi_2}{2}\right) \operatorname{arctanh}\left[\sin\left(\frac{\varphi_2}{2}\right)\right], \quad (5)$$

where  $\Delta_0$  is the zero-temperature superconducting energy gap of the ring.

Figure 1(b) shows the normalized CPR of  $J_2$  [ $I_{J2}(T)/I_{C2,0}$ , with  $I_{C2,0} = \pi \Delta_0/eR_2$  the zero-temperature junction critical current] as a function of  $\varphi_2$  for different temperatures (normalized with respect to the critical temperature  $T_C$ ). By raising  $T$ , the CPR evolves from a skewed to a perfect sinusoidal phase dependence [18,24]. This behavior entails the higher responsivity of  $J_2$  when

the L-SQUIPT is operated at low temperature. Notably, the CPR is almost the same for the  $T = 0$  limit (black squares) and for  $T = 0.01T_C$  (cyan line), as shown in Fig. 1(b).

The resulting temperature-dependent Josephson inductance ( $L_{J2}$ ) of  $J_2$  can be written as

$$L_{J2}(\varphi_2, T) = \frac{\hbar}{2e} \frac{d\varphi_2}{dI_{J2}(\varphi_2, T)}. \quad (6)$$

In the zero-temperature limit, the kinetic inductance can be obtained by substituting Eq. (5) into the above expression. The resulting closed form is therefore

$$\begin{aligned} L_{J2}(\varphi_2, T = 0) &= \frac{I_{C2,0}}{2e} \\ &\times \left[ -\frac{1}{2} \sin\left(\frac{\varphi_2}{2}\right) \operatorname{artanh}\left[\sin\left(\frac{\varphi_2}{2}\right)\right] \right. \\ &\left. + \frac{\cos^2(\varphi_2/2)}{2 - 2 \sin^2(\varphi_2/2)} \right]^{-1}. \end{aligned} \quad (7)$$

Figure 1(c) shows the normalized Josephson inductance  $L_{J2}/L_{J2,0}$  (with  $L_{J2,0}$  its zero-temperature and zero-phase value) as a function of  $\varphi_2$  calculated for different temperatures. At low temperature ( $T \leq 0.3T_C$ ) and for  $\varphi_2 \rightarrow \pi$ , the Josephson inductance drops by about one order of magnitude with respect to  $L_{J2,0}$ . Furthermore, in the limit of  $\varphi_2 \rightarrow \pi$ , the zero-temperature kinetic inductance [see Eq. (7)] goes to zero. As a matter of fact, the vanishing of  $L_{J2}$  does not allow us to efficiently phase bias the Josephson junction in a conventional SQUIPT, since its inductance becomes smaller than that of the ring ( $L_2$ ). As we show below, the L-SQUIPT allows us to exploit the full phase bias of  $J_2$ , yielding largely enhanced transfer functions even at the lowest temperatures, where the magnetometer is expected to show its maximum magnetic flux sensitivity.

To perform the readout operation, the weak link  $J_2$  is equipped with a superconducting readout tunnel probe [ $P$ , green electrode in Fig. 1(a)], as in conventional SQUIPTs [17]. On the one hand, this geometry allows us to operate the magnetometer by conventional quasiparticle transport measurements in both voltage and current bias. On the other hand, the  $\Phi_1$ -dependent Josephson coupling between  $J_2$  and  $P$  can be exploited to design different dissipationless readout schemes for the L-SQUIPT. In particular, the variation of the Josephson output tunnel junction inductance ( $L_{\text{out}}$ ) can be detected by an inductively coupled SQUID readout or by dispersive microwave measurements.

We note that the double-loop structure of the L-SQUIPT resembles the bi-SQUID magnetometer [25,26]. Indeed, the first superconducting loop converts the external magnetic flux into a phase difference across a Josephson junction in both devices. The bi-SQUID is a dc SQUID, thus operating in the Josephson regime only, where a third Josephson junction is introduced to linearize the voltage

response of the device. Differently, in the L-SQUIPT, the second ring is interrupted by a single junction. Furthermore, the readout is performed by means of a tunnel probe sensitive to the modulation of the DOS of  $J_2$ . Indeed, the response of the L-SQUIPT to  $\Phi_1$  is expected to be strongly nonlinear for both the dissipative and dissipationless readouts.

### III. PHASE BIASING $J_2$

The dependence of the phase drop  $\varphi_2$  across  $J_2$  on the external magnetic flux  $\Phi_1$  can be calculated by considering three conditions typical of Josephson interferometers: (i) the quantization of the magnetic flux piercing the first loop; (ii) the phase locking between  $J_1$  and  $J_2$ ; (iii) the circulating supercurrent conservation in the L-SQUIPT double loop.

Thanks to the flux quantization, the phase drop across  $J_1$  is related to  $\Phi_1$  through

$$\varphi_1 + \frac{2\pi L_1}{\Phi_0} I_R = \frac{2\pi \Phi_1}{\Phi_0}, \quad (8)$$

where  $I_R$  is the total supercurrent circulating in the L-SQUIPT. Equation (8) describes the  $\Phi_1 \rightarrow \varphi_1$  conversion by taking into account the finite inductance  $L_1$  of the first superconducting ring necessary to efficiently couple the L-SQUIPT to the external magnetic field. Furthermore, the phase drop  $\varphi_2$  across  $J_2$  is locked to  $\varphi_1$  by the equation

$$\varphi_2 - \varphi_1 + \frac{2\pi L_2}{\Phi_0} I_{J_2} = 0, \quad (9)$$

since the magnetic flux through the second ring is assumed to be zero ( $\Phi_2 = 0$ ). Equation (9) illustrates the  $\varphi_1 \rightarrow \varphi_2$  conversion, which is strongly influenced by the finite inductance of the second ring ( $L_2$ ).

Finally, to calculate the  $\varphi_2(\Phi_1)$  characteristics, we need to consider the conservation of the circulating current in the L-SQUIPT. This implies that  $I_R$  is distributed between the two Josephson junctions  $J_1$  and  $J_2$ , that is,

$$I_R = I_{J_1} + I_{J_2}. \quad (10)$$

As a result, the phase drop across  $J_2$  as a function of the external flux piercing the first loop reads

$$\begin{aligned} \varphi_2 = & \frac{2\pi \Phi_1}{\Phi_0} - \beta \{ \sin [\varphi_2 + \beta \mathcal{L} \mathcal{R} \Xi(\varphi_2)] \\ & + \mathcal{R} \Xi(\varphi_2)(1 + \mathcal{L}) \}, \end{aligned} \quad (11)$$

where  $\beta = (2\pi L_1 I_{C1})/\Phi_0$  is the screening parameter accounting for the finite inductance  $L_1$  of the first loop,

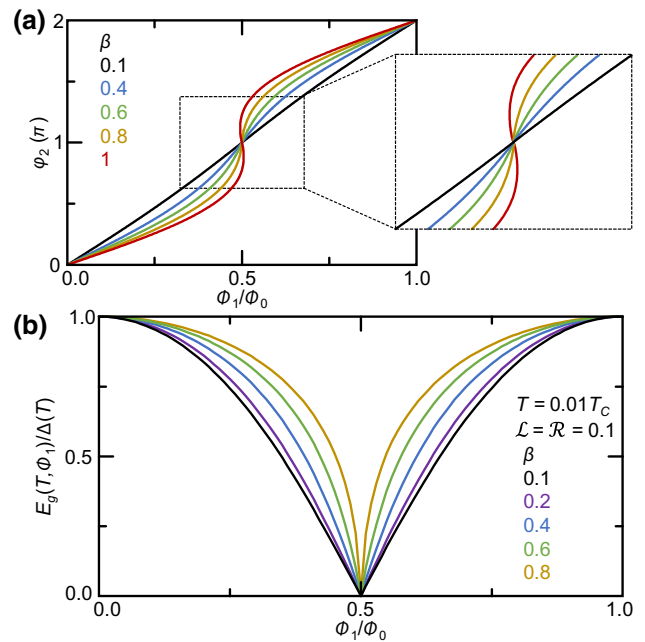


FIG. 2. (a) Phase drop ( $\varphi_2$ ) across  $J_2$  as a function of the external flux  $\Phi_1$  calculated assuming that  $T = 0.01T_C$  and  $\mathcal{L} = \mathcal{R} = 0.1$  for different values of  $\beta$ . Inset: enlargement of the  $\varphi_2$  versus  $\Phi_1$  characteristics calculated around  $\Phi_1 = 0.5\Phi_0$ . (b) Minigap induced in  $J_2$  ( $E_g$ ) as a function of  $\Phi_1$  calculated at  $\mathcal{L} = \mathcal{R} = 0.1$  and  $T = 0.01T_C$  for different values of  $\beta$ .

$\mathcal{L} = L_2/L_1$  describes the difference between the inductance of the two loops, and  $\mathcal{R} = I_{C2,0}/I_{C1,0}$  takes into account the asymmetry in the critical currents of  $J_1$  and  $J_2$ . We note that to have an efficient  $\Phi_1 \rightarrow \varphi_2$  transduction, the ring inductances of the two loops need to satisfy  $L_1 \gg L_2$ , that is  $\mathcal{L} \ll 1$  is required in Eq. (11).

Figure 2(a) shows the  $\varphi_2(\Phi_1)$  characteristics calculated by solving Eq. (11) for different values of  $\beta$  at  $\mathcal{L} = \mathcal{R} = 0.1$  and  $T = 0.01T_C$ . When the inductance of the first loop is large, the phase bias shows a strong nonlinearity with  $\Phi_1$ . In particular,  $\varphi_2$  shows multiple solutions for  $\beta \gtrsim 0.8$  in the flux range  $\Phi_1 \rightarrow 0.5\Phi_0$ , thereby preventing to fully phase bias  $J_2$ . By contrast, for lower values of  $\beta$ , the phase drop is a continuous function of the external magnetic flux; thus,  $J_2$  is sensitive to each value of  $\Phi_1$ . In the following, we use  $\beta = 0.8$  to optimize the phase bias of  $J_2$  and, therefore, to maximize the sensitivity of the L-SQUIPT magnetometer. We note that  $J_2$  shows a vanishing inductance in these conditions, since it operates in the *short-junction* limit and at low temperatures [see Fig. 1(b)]. Therefore, an efficient phase bias of the junction would be impossible in a conventional SQUIPT.

The  $\Phi_1$ -dependent values of  $\varphi_2$  strongly influence the DOS ( $\mathcal{N}_{J2}$ ) of the normal-metal element forming the output Josephson junction. Since  $J_2$  is assumed to be in the

short-junction limit, its DOS takes the form [21,27]

$$\begin{aligned} \mathcal{N}_{J2}(x, \epsilon, \varphi_2) = & \text{Re} \sqrt{\frac{(\epsilon + i\Gamma)^2}{(\epsilon + i\Gamma)^2 - \Delta^2(T) \cos^2(\varphi_2/2)}} \\ & \times \cosh \left( \frac{2x - L}{L} \text{arccosh} \right. \\ & \left. \sqrt{\frac{(\epsilon + i\Gamma)^2 - \Delta^2(T) \cos^2(\varphi_2/2)}{(\epsilon + i\Gamma)^2 - \Delta^2(T)}} \right), \quad (12) \end{aligned}$$

where  $\epsilon$  is the energy relative to the chemical potential of the superconductors,  $\Gamma$  is the Dynes broadening parameter [28], and  $x \in [0, L]$  is the spatial coordinate along the  $J_2$  length. Equation (12) highlights that the density of states is strongly tuned by  $\varphi_2$ . In particular, superconducting minigap induced in the normal metal by the proximity to the superconductor [14] takes the form

$$E_g(T, \varphi_2) = \Delta(T) \cos \left( \frac{\varphi_2}{2} \right). \quad (13)$$

We note that the value of  $E_g$  is constant along the nanowire length. For  $\varphi_2 = 0$ , the induced minigap is maximum [ $E_g(T, 0) = \Delta(T)$ ], while for  $\varphi_2 = \pi$ , the nanowire shows the normal-metal DOS [ $E_g(T, \pi) = 0$ ].

In the L-SQUIPT, the dependence of the minigap on the external magnetic flux [ $E_g(T, \Phi_1)$ ] can be calculated by combining Eqs. (11) and (13). Figure 2(b) presents the dependence of  $E_g(T)$  on  $\Phi_1$  calculated at  $T = 0.01T_C$  and  $\mathcal{L} = \mathcal{R} = 0.1$  for different values of  $\beta$ . By enhancing the screening parameter, the minigap shows a stronger variation with external magnetic flux at  $\Phi_1 \rightarrow 0.5\Phi_0$ . On the contrary, the minigap is more sensitive at  $\Phi_1 \rightarrow \Phi_0$  for low values of  $\beta$ , but its maximum steepness is limited. Therefore, the L-SQUIPT magnetometer is expected to show higher sensitivity for large values of  $\beta$  at  $\Phi_1 \rightarrow 0.5\Phi_0$ .

#### IV. DISSIPATIVE READOUT

Here, we discuss the magnetic-flux-dependent quasiparticle transport between  $J_2$  and  $P$ . This will allow us to evaluate the sensitivity of the L-SQUIPT magnetometer both in the voltage bias and current bias configurations.

##### A. Quasiparticle transport

The quasiparticle current flowing through the  $J_2$ - $P$  tunnel junction can be written as [17]

$$\begin{aligned} I_{qp} = & \frac{1}{ewR_T} \int_{(L-w)/2}^{(L+w)/2} dx \int_{-\infty}^{\infty} d\epsilon \mathcal{N}_{J2}(x, \epsilon, \varphi_2) \\ & \times \mathcal{N}_p(\epsilon, V) \mathcal{F}(\epsilon, V), \quad (14) \end{aligned}$$

where  $R_T$  and  $w$  are the normal-state resistance and the width of the junction, respectively. Furthermore,

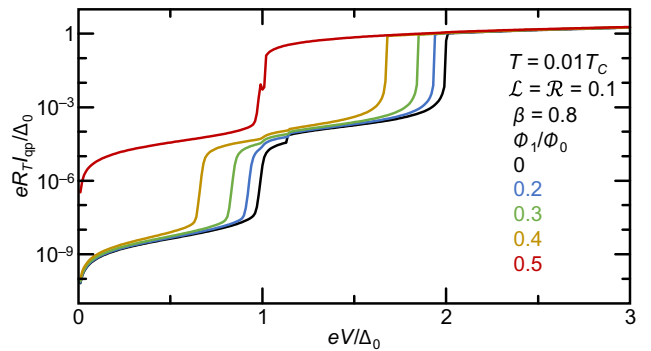


FIG. 3. Quasiparticle current as a function of voltage calculated at  $\beta = 0.8$  for  $\mathcal{L} = \mathcal{R} = 0.1$ ,  $T = 0.01T_C$  and several values of  $\Phi_1$ . For all curves,  $\Gamma = 10^{-4}\Delta_0$ .

$\mathcal{F}(\epsilon, V) = [f_0(\epsilon - eV) - f_0(\epsilon)]$  is the difference between the Fermi-Dirac distribution functions ( $f_0$ ) of the two electrodes. The normalized Bardeen-Cooper-Schrieffer DOS of the superconducting tunnel probe can be written as

$$\mathcal{N}_p(\epsilon, V) = \left| \text{Re} \left[ \frac{(\epsilon - eV + i\Gamma)}{\sqrt{(\epsilon - eV + i\Gamma)^2 - \Delta^2(T)}} \right] \right|. \quad (15)$$

For simplicity, we assume that  $P$  is made of the same superconductor as the L-SQUIPT ring.

The typical quasiparticle current ( $I_{qp}$ ) versus voltage ( $V$ ) characteristics of the L-SQUIPT calculated at  $\beta = 0.8$  for  $\mathcal{L} = \mathcal{R} = 0.1$  and  $T = 0.01T_C$  are shown in Fig. 3 for several values of the external magnetic flux. The quasiparticle current tunnels through the barrier when the voltage bias is larger than the sum of the energy gaps of  $J_2$  and  $P$ , that is, for  $eV \geq \Delta(T) + E_g(T, \Phi_1)$  [29]. Indeed, the threshold voltage is maximal for  $\Phi_1 = 0$  (black curve), since the minigap in the normal metal acquires the same value of the energy gap of the superconducting ring [ $E_g(T, 0) = \Delta(T)$ ]. By raising the external magnetic flux, large quasiparticle tunneling occurs at lower values of voltage bias until reaching its minimum value  $eV = \Delta(T)$  for  $\Phi_1 = 0.5\Phi_0$  [red curve, since  $E_g(T, 0.5\Phi_0) = 0$ ]. The variation of the  $I_{qp}(V)$  characteristics with the magnetic flux is stronger in the interval  $0.4\Phi_0 \leq \Phi_1 \leq 0.5\Phi_0$ , since  $E_g$  shows a stark dependence on  $\Phi_1$  in this range [see Fig. 2(b)]. As a consequence, the L-SQUIPT can be operated as a sensitive magnetometer by simple measurements of the output junction voltage in current bias mode or the tunneling quasiparticle current in voltage bias.

##### B. Voltage bias operation

The voltage bias operation of the L-SQUIPT magnetometer takes advantage of the strong  $\Phi_1$  dependence of  $I_{qp}$  for specific values of  $V$ , as shown in Fig. 4(a). In particular, the current is almost independent of the magnetic flux for  $V = 2\Delta_0/e$ , since the output junction is always biased

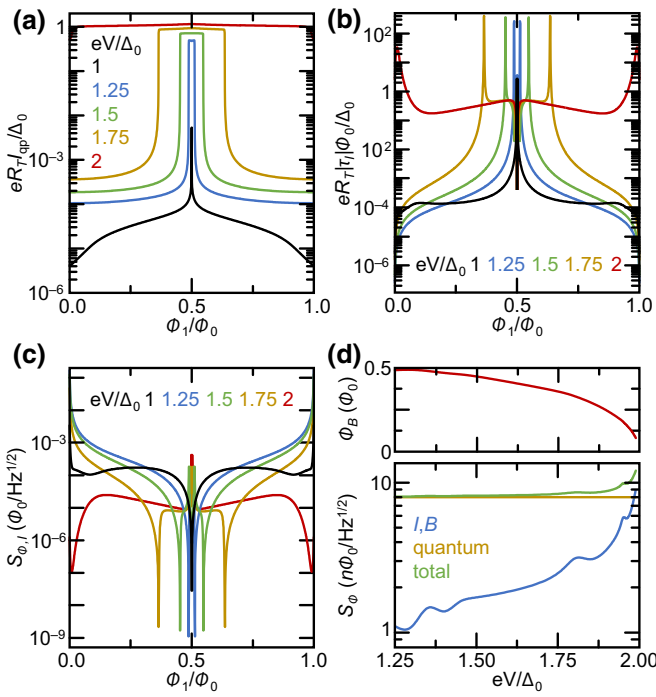


FIG. 4. Voltage bias operation. (a) Quasiparticle current as a function of the external magnetic flux calculated for several values of  $V$ . (b) Flux-to-current transfer function versus  $\Phi_1$  calculated for different values of the bias voltage. (c) Flux sensitivity per unit bandwidth as a function of  $\Phi_1$  for different values of  $V$ . In the calculations we set  $R_T = 50 \text{ k}\Omega$  and  $\Delta_0 = 200 \mu\text{eV}$ . (d) Top: magnetic flux corresponding to the best sensitivity versus  $V$ . Bottom: best flux sensitivity per unit bandwidth (blue) and quantum noise (gold) versus  $V$ . The total sensitivity is shown in green. For all panels,  $\beta = 0.8$ ,  $\mathcal{L} = \mathcal{R} = 0.1$ ,  $T = 0.01T_C$ , and  $\Gamma = 10^{-4}\Delta_0$ .

in the normal state. For lower values of the bias voltage, the modulation of  $E_g$  with  $\Phi_1$  results in the strong variation of  $I_{qp}$  with the magnetic flux. Indeed, by decreasing  $V$  the maximum steepness of the curves moves towards  $\Phi_1 = 0.5\Phi_0$ , which is reached for  $V = \Delta_0/e$ , thus corresponding to  $E_g(\Phi_1) = 0$  [see Fig. 2(b)]. As a consequence, the voltage bias operation of the L-SQUIPT requires  $\Delta_0 < eV < 2\Delta_0$ .

The  $\Phi_1$  dependence of  $I_{qp}$  is completely reflected in the flux-to-current transfer function, which is defined as

$$\tau_I = \frac{dI_{qp}}{d\Phi_1}. \quad (16)$$

Figure 4(b) shows  $\tau_I$  versus  $\Phi_1$  calculated for the same parameters as  $I_{qp}$  [panel (a)]. At a given  $V$ , the maximum value of the transfer function corresponds to the strongest variation of  $I_{qp}$  with  $\Phi_1$ , while  $\tau_I = 0$  for  $\Phi_1 = 0.5\Phi_0$  [where  $I_{qp}$  shows its maximum; see Fig. 4(a)].

The most common figure of merit for a magnetometer is the flux noise, i.e., the flux sensitivity per unit bandwidth.

In the voltage bias operation, this can be written as

$$S_{\Phi,I} = \frac{\sqrt{S_I}}{|\tau_I|}, \quad (17)$$

where  $S_I$  is the current-noise spectral density. The latter reads

$$S_I = 2eI_{qp}(V) \coth(eV/2k_B T). \quad (18)$$

Figure 4(c) shows the  $\Phi_1$  dependence of  $S_{\Phi,I}$  for the L-SQUIPT calculated at different values of the bias voltage. For these simulations, we assume a geometry and materials feasible by standard fabrication techniques. Indeed, we set  $\Delta_0 = 200 \mu\text{eV}$  (aluminum) for the superconducting ring and the output tunnel probe, while considering a tunnel resistance  $R_T = 50 \text{ k}\Omega$ . The flux sensitivity strongly depends on both  $\Phi_1$  and  $V$ . Indeed, depending on the magnetic flux of interest, the best operating point ( $\Phi_B$ ) can be chosen by tuning the bias voltage [see the top panel of Fig. 4(d)]. The flux noise corresponding to  $\Phi_B$  is  $S_{\Phi,I_{best}} < 10 \text{ n}\Phi_0/\sqrt{\text{Hz}}$  for a bias voltage in the range  $1.25\Delta_0 \leq eV < 2\Delta_0$ . We note that, in a superconducting interferometer, the ultimate flux sensitivity is limited by the quantum noise ( $S_{\Phi,q}$ ) defined as [30]

$$S_{\Phi,q} = \sqrt{\hbar L_1}. \quad (19)$$

By substituting  $I_{C1} = 100 \mu\text{A}$  into the screening parameter equation, we obtain  $L_1 = 2.6 \text{ pH}$ . The resulting quantum noise due to the inductance of the superconducting ring is  $S_{\Phi,q} = 8 \text{ n}\Phi_0/\sqrt{\text{Hz}}$ . Therefore, the L-SQUIPT magnetometer operated in voltage bias shows a quantum limited flux sensitivity for most values of  $V$ . In fact,  $S_{\Phi,q}$  dominates the total flux noise of the device, defined as  $S_{\Phi,t} = \sqrt{s_{\Phi,t}^2 + S_{\Phi,q}^2}$ , in almost the full voltage range [see the bottom panel of Fig. 4(d)]. Furthermore, this L-SQUIPT geometry guarantees a best magnetic field sensitivity  $S_{B,t} = S_{\Phi,t}/A_1 = 1.1 \text{ pT}/\sqrt{\text{Hz}}$ , where  $A_1 = 14 \mu\text{m}^2$  is the area of the first loop. We note that the value of  $A_1$  is obtained by considering a circular loop of radius  $R_1 = L_1/\mu_0$  (with  $\mu_0 = 4\pi \times 10^{-7} \text{ H/m}$  the magnetic permeability of vacuum).

### C. Current bias operation

The current bias operation of the L-SQUIPT magnetometer exploits the dependence of  $V$  on  $\Phi_1$  while a constant  $I_{qp}$  is injected in the device, as shown in Fig. 5(a). For  $I_{qp} = \Delta_0/(eR_T)$ , the modulation of  $V$  with the external magnetic flux is limited, while, by decreasing the bias current, the voltage span and the steepness of the

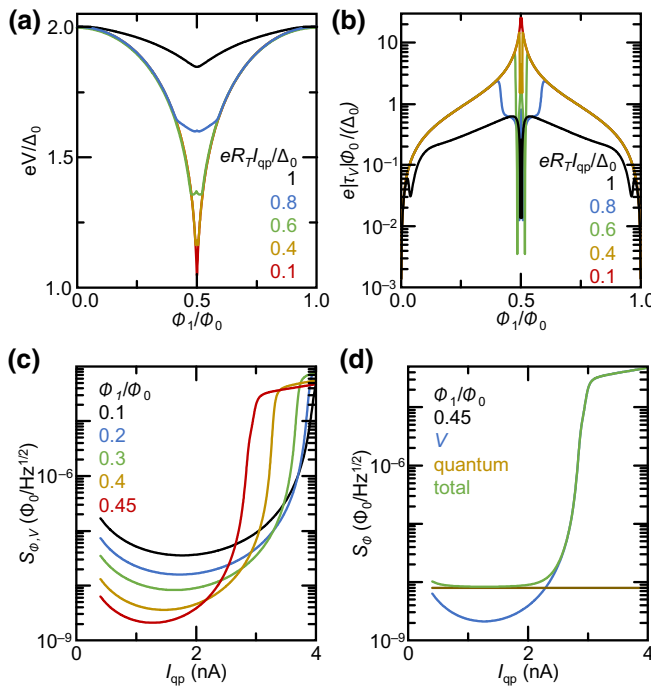


FIG. 5. Current bias operation. (a) Output voltage as a function of the external magnetic flux calculated for several values of  $I_{qp}$ . (b) Flux-to-voltage transfer function versus  $\Phi_1$  calculated for different values of the bias current. (c) Flux sensitivity per unit bandwidth as a function of  $I_{qp}$  for different values of  $\Phi_1$ . In the calculations we set  $R_T = 50 \text{ k}\Omega$  and  $\Delta_0 = 200 \mu\text{eV}$ . (d) Flux sensitivity per unit bandwidth (blue) and quantum noise (gold) versus  $I_{qp}$  calculated for  $\Phi_1 = 0.45\Phi_0$ . The total sensitivity is shown in green. For all panels,  $\beta = 0.8$ ,  $\mathcal{L} = \mathcal{R} = 0.1$ ,  $T = 0.01T_C$ , and  $\Gamma = 10^{-4}\Delta_0$ .

curves increase. This behavior is highlighted by the flux-to-voltage transfer function

$$\tau_V = \frac{dV}{d\Phi_1}. \quad (20)$$

Indeed, the maximum value of the transfer function rises while moving towards  $0.5\Phi_0$  by increasing the bias current [see Fig. 5(b)]. In particular, the L-SQUIPT shows  $\tau_V \simeq 26\Delta_0/(e\Phi_0)$  at  $\Phi_1 = 0.498\Phi_0$  for  $I_{qp} = 0.1\Delta_0/(eR_T)$ .

In the current bias operation, the flux sensitivity per unit bandwidth can be written as

$$S_{\Phi,V} = \frac{\sqrt{S_V}}{|\tau_V|}, \quad (21)$$

where the voltage-noise spectral density takes the form

$$S_V = R_d^2 S_I = \left( \frac{dV}{dI} \right)^2 S_I. \quad (22)$$

In the above equation,  $R_d = dV/dI$  is the differential resistance of the output Josephson junction. Figure 5(c) shows

$S_{\Phi,V}$  as a function of  $I_{qp}$  for several values of  $\Phi_1$ . For the simulations, we consider the same structure as the voltage bias configuration, that is,  $\Delta_0 = 200 \mu\text{eV}$  for both the superconducting ring and the output tunnel electrode ( $R_T = 50 \text{ k}\Omega$ ). The L-SQUIPT sensitivity is maximum for high values of magnetic flux, as a result of the increased flux-to-voltage transfer function [see Fig. 5(b)]. In particular, a flux sensitivity of about  $2 n\Phi_0/\sqrt{\text{Hz}}$  can be reached for  $\Phi = 0.45\Phi_0$  at  $I_{qp} \simeq 1.3 \text{ nA}$ .

Also in the current bias mode, the L-SQUIPT magnetometer shows a quantum limited flux sensitivity. Indeed,  $S_{\Phi,q} = 8 n\Phi_0/\sqrt{\text{Hz}}$  dominates the total flux noise of the device in a wide range of bias currents, as shown in Fig. 5(d) for  $\Phi = 0.45\Phi_0$ .

#### D. Temperature dependence

Here, we investigate the temperature dependence of the L-SQUIPT performance both in voltage and in current bias. To this end, we set the same device parameters as in previous sections, that is,  $\mathcal{L} = \mathcal{R} = 0.1$ ,  $\Gamma = 10^{-4}\Delta_0$ ,  $R_T = 50 \text{ k}\Omega$ , and  $\Delta_0 = 200 \mu\text{eV}$ . Since  $\beta$  is a temperature-dependent parameter, we consider  $\beta(T = 0.01T_C) = 0.8$ , taking into account the exponential damping of  $I_{C1}$  with  $T$  [18]. Indeed, Eq. (2) can be employed for  $T \geq 0.05T_C$  in an aluminum/copper SNS junction of length  $L = 2 \mu\text{m}$  (with  $D = 6 \times 10^{-3} \text{ m}^2/\text{s}$  the diffusion coefficient of copper).

Figure 6(a) shows the flux sensitivity in the voltage bias operation (at  $V = 1.25\Delta_0/e$ ) as a function of  $\Phi_1$  calculated for different values of  $T$ . By increasing the temperature, the best value of  $S_{\Phi,I}$  rises substantially, while  $\Phi_B$  is only slightly affected by  $T$ . On the contrary, the sensitivity far away from the best operating point improves by increasing the temperature, since the flux-to-current transfer function shows a smoother dependence in  $\Phi_1$ . Indeed, at high temperature, the CPR of  $J_2$  shows a lower slope around  $\varphi_2 = \pi$  [see Fig. 1(b)], thus causing a smaller variation of  $I_{qp}$  with  $\Phi_1$ . This degrades the best performance of the L-SQUIPT, but it provides a more constant sensitivity in the whole magnetic flux range [see the red curve in Fig. 6(a)].

Figure 6(b) shows the temperature dependence of the flux sensitivity of the L-SQUIPT operated in current bias at  $\Phi_1 = 0.45\Phi_0$ . By raising the temperature, the best sensitivity of the magnetometer is slightly affected by temperature, but the range of bias current showing high sensitivity narrows. For  $T = 0.5T_C$ , a flux sensitivity  $S_{\Phi,V} \sim 10 n\Phi_0/\sqrt{\text{Hz}}$  is obtained for  $I_{qp} \sim 1 \text{ nA}$ . Thus, the L-SQUIPT is a quantum limited magnetometer both in voltage and current bias operations only for  $T < 0.5T_C$ .

#### V. DISSIPATIONLESS READOUT

Here, we discuss the magnetic-flux-dependent Josephson transport between  $J_2$  and  $P$ . This will allow us to evaluate the sensitivity of the L-SQUIPT magnetometer in different dissipationless readout geometries.

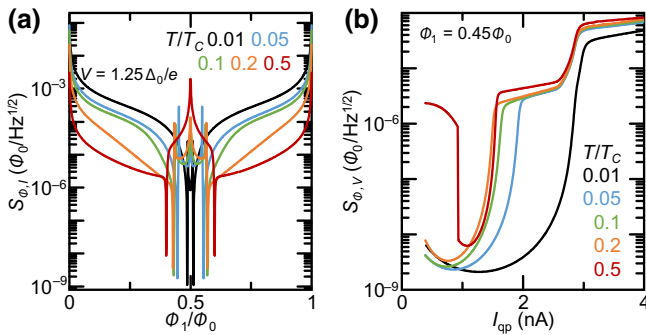


FIG. 6. Temperature dependence of the flux sensitivity. (a) Flux sensitivity per unit bandwidth as a function of  $\Phi_1$  for different temperatures calculated at  $V = 1.25\Delta_0/e$ . (b) Flux sensitivity per unit bandwidth as a function of  $I_{\text{qp}}$  calculated for different temperatures at  $\Phi_1 = 0.45\Phi_0$ . For all panels,  $\beta = 0.8$ ,  $\mathcal{L} = \mathcal{R} = 0.1$ ,  $\Gamma = 10^{-4}\Delta_0$ ,  $R_T = 50\text{ k}\Omega$ , and  $\Delta_0 = 200\text{ }\mu\text{eV}$ .

### A. Josephson current and inductance

Since we assume a superconducting tunnel readout probe, a dissipationless zero-bias current ( $I_{\text{out}}$ ) can flow thanks to Josephson coupling. The latter can be calculated by means of  $I_{\text{out}} = I_{C,\text{out}} \sin(\varphi_{\text{out}})$ , where  $I_{C,\text{out}}$  is the critical current of the junction and  $\varphi_{\text{out}}$  the phase difference between the tunnel probe and  $J_2$ . The critical current can be calculated through the Ambegaokar-Baratoff equation for a pointlike junction [17,31]

$$I_{C,\text{out}}(T, \varphi_2) = \frac{\pi E_g(T, \varphi_2) \Delta(T) k_B T}{e R_T} \times \sum_{l=0, \pm 1, \dots} \frac{1}{\sqrt{[\omega_l^2 + E_g^2(T, \varphi_2)][\omega_l^2 + \Delta^2(T)]}}, \quad (23)$$

where  $\omega_l = \pi k_B T(2l + 1)$ .

Figure 7(a) shows  $I_{\text{out}}$  versus  $\Phi_1$  calculated for an L-SQUIPT at  $T = 0.01 T_C$  and  $\mathcal{L} = \mathcal{R} = 0.1$  for different values of  $\beta$  by assuming that  $\varphi_{\text{out}} = \pi/2$ . We consider the same structure as in the previous calculations, that is,  $\Delta_0 = 200\text{ }\mu\text{eV}$  and  $R_T = 50\text{ k}\Omega$ . At  $\Phi_1 = 0$ , all the curves collapse to the maximal output junction critical current (about 6.2 nA). By raising the external magnetic flux,  $I_{\text{out}}$  lowers until reaching its minimum at  $\Phi_1 = 0.5\Phi_0$ , because the superconducting energy gap of  $J_2$  closes. The energy gap shows a steeper dependence on  $\Phi_1$  for large values of  $\beta$  [see Fig. 2(b)]. This behavior is transferred to the Josephson current. Indeed, the variation of  $I_{\text{out}}$  around  $\Phi_1 = 0.5\Phi_0$  is less sharp for low values of the screening parameter [see Fig. 7(a)].

The suppression of the critical current causes the variation of the Josephson inductance of the readout junction ( $L_{J_{\text{out}}}$ ). The latter can be calculated by substituting  $I_{\text{out}}$  into Eq. (6). Consequently,  $L_{J_{\text{out}}}$  is only proportional to

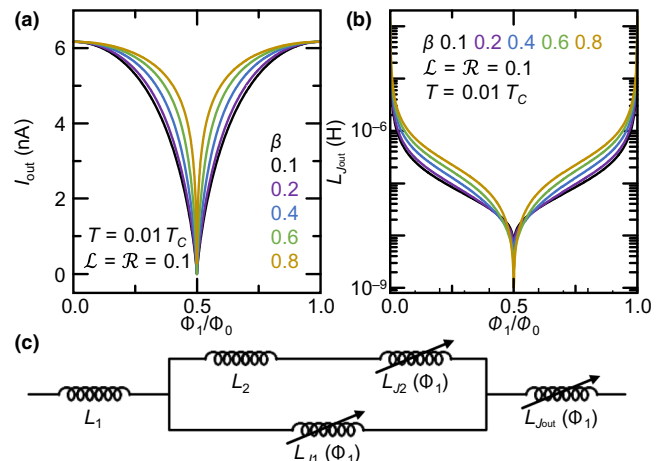


FIG. 7. Josephson transport through the readout junction. (a) Josephson current flowing through the output tunnel junction as a function of  $\Phi_1$  calculated for different values of  $\beta$ . (b) Kinetic inductance of the output tunnel junction as a function of  $\Phi_1$  calculated for different values of  $\beta$ . In both panels,  $\mathcal{L} = \mathcal{R} = 0.1$ ,  $\Gamma = 10^{-4}\Delta_0$ ,  $T = 0.01 T_C$ ,  $R_T = 50\text{ k}\Omega$ ,  $\Delta_0 = 200\text{ }\mu\text{eV}$ , and  $\varphi_{\text{out}} = \pi/2$ . (c) Schematic representing all the components of the total inductance ( $L_{\text{TOT}}$ ) of the L-SQUIPT. We represent all the inductance contributions that directly or indirectly depend on  $\Phi_1$ .

the derivative of  $\varphi_2$  with respect to  $I_{\text{out}}$ , since we assumed that  $\varphi_{\text{out}} = \pi/2$ . Figure 7(b) shows  $L_{J_{\text{out}}}$  versus  $\Phi_1$  calculated starting from the Josephson currents shown in panel (a). For all values of  $\beta$ , the inductance spans over several orders of magnitude. By increasing  $\beta$ , the overall variation of  $L_{J_{\text{out}}}$  with the magnetic flux increases and its maximum steepness moves from  $\Phi_1 \rightarrow 0$  to  $\Phi_1 \rightarrow 0.5\Phi_0$ .

For the implementation of dissipationless readout schemes, we need to consider the total inductance of the L-SQUIPT ( $L_{\text{TOT}}$ ). The different inductances are connected in series if they sustain the same current flow; otherwise, they are connected in parallel (the current divides between the different arms). The resulting schematic representation of  $L_{\text{TOT}}$  is shown in Fig. 7(c). Here, the small ring inductance  $L_2$  and the second junction inductance  $L_{J_2}$  are in series. This block is in parallel with the inductance ( $L_{J_1}$ ) of junction  $J_1$ . The resulting inductance is in series with the large loop inductance  $L_1$ . All these are in series with the Josephson output tunnel junction inductance  $L_{\text{out}}$ . Thus, the total inductance is

$$L_{\text{TOT}}(\Phi_1) = L_1 + \frac{L_{J_1}(\Phi_1)[L_2 + L_{J_2}(\Phi_1)]}{L_2 + L_{J_1}(\Phi_1) + L_{J_2}(\Phi_1)} + L_{J_{\text{out}}}(\Phi_1). \quad (24)$$

The variation in the Josephson inductance, and thus  $L_{\text{TOT}}$ , can be revealed through different dissipationless readout schemes. Indeed, the L-SQUIPT can be inductively coupled to a SQUID amplifier, as routinely realized for kinetic inductance detectors (KIDs). Alternatively, the device can

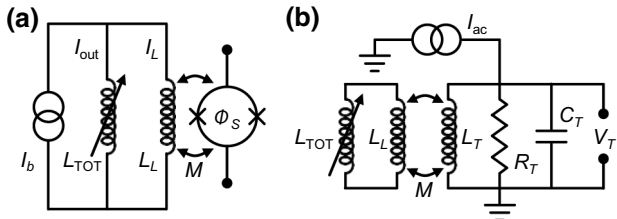


FIG. 8. Dissipationless readouts for the L-SQUIPT. (a) Inductive readout scheme, where the changes in the L-SQUIPT inductance ( $L_{\text{TOT}}$ ) are recorded by a dc SQUID magnetometer coupled to the device by a mutual inductance  $M$ . (b) Dispersive readout scheme, where the changes in  $L_{\text{TOT}}$  are recorded thanks to the changes in the characteristic frequency of a resonant circuit inductively coupled to the L-SQUIPT.

be integrated in a  $RLC$  resonant circuit, whose resonance frequency varies with  $\Phi_1$ .

### B. Inductive readout

The scheme for the inductive readout of the L-SQUIPT is shown in Fig. 8(a). The parallel connection of the L-SQUIPT (of inductance  $L_{\text{TOT}}$ ) and a load inductor ( $L$ ) is biased by means of a dc current generator ( $I_b$ ). Indeed, the variation of  $L_{\text{TOT}}$  generates a change in the current flowing through the L-SQUIPT ( $I_{\text{out}}$ ) and the load resistor ( $I_L$ ). The latter is detected by a dc SQUID inductively coupled to the circuit through the mutual inductance  $M$ , where the magnetic flux piercing the SQUID is  $\Phi_s = MI_L$ . For small variations of  $\Phi_s$  (linear response regime,  $LI_L \ll \Phi_0$ ) [32], the current flowing through the load inductor reads

$$I_L = I_b \frac{\Phi_0}{\Phi_0 + 2\pi LI_{\text{out}}}. \quad (25)$$

In this configuration, the L-SQUIPT operates as a magnetic-flux-to-magnetic-flux transducer or magnetic flux amplifier, where the efficiency can be quantified by

$$\frac{d\Phi_s}{d\Phi_1} = \frac{dI_{\text{out}}}{d\Phi_1} M \frac{dI_L}{dI_{\text{out}}}. \quad (26)$$

The ratio  $dI_{\text{out}}/d\Phi_1$  can be calculated through the derivative of Eq. (23) with respect of the input magnetic flux. Accordingly, the term  $dI_L/dI_{\text{out}}$  can be calculated by performing the  $dI_{\text{out}}$  derivative of Eq. (25), thus obtaining

$$\frac{dI_L}{dI_{\text{out}}} = 2\pi LI_b \frac{\Phi_0}{(\Phi_0 + 2\pi LI_{\text{out}})^2}. \quad (27)$$

### C. Dispersive measurement

The scheme for the dispersive readout of the L-SQUIPT is shown in Fig. 8(b), where the  $\Phi_1$ -dependent variation

of the Josephson inductance  $L_{\text{out}}$  is determined by measuring the resonance frequency of a suited  $RLC$  circuit. To this end, a load inductance  $L_L$  is added in parallel to the total inductance of the L-SQUIPT ( $L_{\text{TOT}}$ ). This circuit is coupled by a mutual inductance ( $M$ ) with a tank circuit characterized by inductance  $L_T$ , capacitance  $C_T$ , and resistance  $R_T$ . The resulting effective inductance of the tank circuit is [33,34]

$$\tilde{L}_T = L_T \left( 1 - \frac{M^2}{L_T} \frac{1}{L_{\text{TOT}}(\Phi_1) + L_L} \right). \quad (28)$$

As a consequence, the resonance frequency of the tank circuit  $\tilde{f}_T = 1/2\pi\sqrt{\tilde{L}_T C_T}$  strongly depends on the flux  $\Phi_1$ .

### D. L-SQUIPT noise in dissipationless readout operation

We assume that the readout circuit in Fig. 8 has negligible noise so that the overall sensitivity of L-SQUIPT is determined by its intrinsic noise associated with each element of the device and their correlations.

From Fig. 8 we can see that noise is essentially determined by the fluctuations of the current across the load inductance  $L_L$  that is then coupled by mutual inductance with the readout circuit. The current of interest is the tunnel junction one  $I_{\text{out}}$  in Eq. (23). This is composed of a Johnson thermal contribution (related to the resistances of Josephson junctions) and a phase contribution.

The Johnson thermal contribution is dominated by the tunnel resistance  $R_T$  that is much larger than  $R_{J_1}$  and  $R_{J_2}$ . For a frequency bandwidth  $\delta\omega/(2\pi)$ , it generates a squared mean noise voltage [33]

$$\langle \delta V_{J_{\text{out}}}^2 \rangle = 4k_B T R_T \frac{\delta\omega}{2\pi}. \quad (29)$$

The tunnel junction can be represented by a  $RLC$  parallel circuit with resistance  $R_T$ , a Josephson inductance  $L_{J_{\text{out}}}$ , and a small capacitance  $C_{\text{out}}$ . Passing to the frequency-dependent impedances, i.e.,  $Z_{R_T} = R_T$ ,  $Z_{L_{J_{\text{out}}}} = i\omega L_{J_{\text{out}}}$ , and  $Z_{C_{\text{out}}} = 1/(i\omega C_{\text{out}})$ , for the junction  $J_{\text{out}}$ , we have an impedance

$$\frac{1}{Z_{J_{\text{out}}}} = \frac{1}{Z_{R_T}} + \frac{1}{Z_{L_{J_{\text{out}}}}} + \frac{1}{Z_{C_{J_{\text{out}}}}}. \quad (30)$$

As a consequence, the mean square of the current noise due to the resistance can be written as [33,35]

$$\langle \delta I_{\text{out},R}^2 \rangle = \frac{\langle \delta V_{J_{\text{out}}}^2 \rangle}{|Z_{J_{\text{out}}}|^2} = \frac{4k_B T R_T \delta\omega}{|Z_{J_{\text{out}}}|^2} \frac{2\pi}{2\pi}. \quad (31)$$

The phase noise contribution to  $I_{\text{out}}$  is due to the fact that, as seen in Eq. (23),  $I_{\text{out}}$  depends on the phase  $\varphi_2$ . To calculate it, we first consider the Johnson noise generated by the

two separate junctions  $J_1$  and  $J_2$  at temperature  $T$ . Analogously to that for the tunnel junction, we find that the noise is

$$\langle \delta I_{J_i}^2 \rangle = \frac{\langle \delta V_{J_i}^2 \rangle}{|Z_{J_i}|^2} = \frac{4k_B T R_{J_i}}{|Z_{J_i}|^2} \frac{\delta\omega}{2\pi} \quad (32)$$

with  $Z_{J_i}$ ,  $i = 1, 2$ , obtained by Eq. (30) with the index exchanges.

These uncorrelated noise sources are combined in the following way. The small loop can be treated as a SQUID with two Josephson junctions in parallel. Following Ref. [33], we consider the circulating current  $I_{\text{circ}}$  as a function of the current flowing through junctions  $J_1$  and  $J_2$ :  $I_{\text{circ}} = I_{J_1} - I_{J_2}$ .

The fluctuations of the circular current coupled with the loop impedance  $L_2$  determine the phase fluctuations  $\delta\varphi_2$ . They can be written as  $\langle \delta I_{\text{circ}}^2 \rangle = \langle \delta I_{J_1}^2 \rangle + \langle \delta I_{J_2}^2 \rangle$ . By multiplying this expression by  $4\pi^2 L_2^2 / \Phi_0^2$  and using Eq. (32), we obtain the mean square of the phase noise

$$\langle \delta\varphi_2^2 \rangle = \frac{16\pi^2 k_B T L_2^2}{\Phi_0^2} \left( \frac{R_{J_1}}{|Z_{J_1}|^2} + \frac{R_{J_2}}{|Z_{J_2}|^2} \right) \frac{\delta\omega}{2\pi}. \quad (33)$$

The noise current of the tunnel junction is the sum of the square of the thermal and phase noise [Eqs. (31) and (33), respectively]

$$\langle \delta I_{\text{out}}^2 \rangle = \frac{4k_B T R_T}{|Z_{J_{\text{out}}}|^2} \frac{\delta\omega}{2\pi} + c_{\varphi_2} \langle \delta\varphi_2^2 \rangle. \quad (34)$$

The coefficient  $c_{\varphi_2}$  is obtained from Eqs. (13) and (23) by taking a small variation of  $I_{\text{out}}$  as a function of  $\varphi_2$ :

$$c_{\varphi_2} = \frac{1}{4} \left( \frac{\pi \Delta^2(T) k_B T}{e R_T} \right)^2 \sin^2 \left( \frac{\varphi_2}{2} \right) \times \left[ \sum_l \frac{1}{\sqrt{[\omega_l^2 + E_g^2(T, \varphi_2)][\omega_l^2 + \Delta^2(T)]}} \right]^2. \quad (35)$$

Finally, the current fluctuations across  $L_L$  induce flux fluctuations

$$\langle \delta\Phi_L^2 \rangle = \langle \delta I_{\text{out}}^2 \rangle L_L^2. \quad (36)$$

This is the intrinsic magnetic flux noise of the L-SQUIPT that is the ultimate limit of the sensitivity of the measurement through the readout circuit in Fig. 8.

We note that the performance for the dissipationless readout of an L-SQUIPT depends nontrivially on  $R_T$ ,  $\delta\omega$ , and  $\Phi_1$ . On the one hand, increasing  $R_T$  and  $\delta\omega$  increases both contributions of  $\langle \delta I_{\text{out}}^2 \rangle$  [see Eq. (34)]. On the other hand, large values of  $R_T$  and  $\delta\omega$  increase  $Z_{J_{\text{out}}}$  [see Eq. (30)], thus suppressing the current noise. Similarly,  $\Phi_1$  acts

on several quantities in Eq. (34) with unexpected consequences. In particular, the noise is minimum for  $\Phi_1 \rightarrow 0$  ( $\varphi_2 \rightarrow 0$ ), since the phase noise contribution becomes negligibly small, as shown by Eq. (35). The best magnetic flux fluctuation for an L-SQUIPT operated in the dissipationless mode is  $\langle \delta\Phi_L \rangle \sim 4 \mu\Phi_0$  obtained at  $\Phi_1 = 0$  for  $\mathcal{L} = \mathcal{R} = 0.1$ ,  $\Gamma = 10^{-4} \Delta_0$ ,  $T = 20$  mK,  $R_T = 50$  kΩ,  $\Delta_0 = 200$  μeV,  $\delta\omega/2\pi = 100$  MHz,  $C_{J_{\text{out}}} = 1$  fF, and  $L_L = 10$  pH.

## VI. CONCLUSIONS

In conclusion, we have proposed and theoretically investigated an innovative highly sensitive magnetometer: the inductive superconducting quantum interference proximity transistor (L-SQUIPT). The L-SQUIPT promises enhanced performance with respect to widespread SQUID and SQUIPT magnetometers. Indeed, an L-SQUIPT made of conventional materials (such as aluminum and copper) would show a quantum limited intrinsic noise down to about  $8 n\Phi_0/\sqrt{\text{Hz}}$ , both in current and voltage bias operations. Furthermore, the superconducting output probe allows us to design two different dissipationless readout schemes based on the variation of the Josephson inductance of the tunnel junction, such as inductive and dispersive readout setups. In these configurations, the best flux fluctuation is  $\langle \delta\Phi_L \rangle \sim 4 \mu\Phi_0$  for a bandwidth of 100 MHz.

## ACKNOWLEDGMENTS

We thank A. Ronzani for useful discussions. The authors acknowledge the European Research Council under Grant Agreement No. 899315 (TERASEC), and the EU's Horizon 2020 research and innovation program under Grants Agreement No. 800923 (SUPERTED) and No. 964398 (SUPERGATE) for partial financial support.

- 
- [1] R. Cantor and D. Koelle, in *The SQUID Handbook* (John Wiley & Sons, Ltd, 2004) Chap. 5, p. 171.
  - [2] R. C. Jaklevic, J. Lambe, A. H. Silver, and J. E. Mercereau, Quantum Interference Effects in Josephson Tunneling, *Phys. Rev. Lett.* **12**, 159 (1964).
  - [3] D. Vasyukov, Y. Anahory, L. Embo, D. Halbertal, J. Cuppens, L. Neeman, A. Finkler, Y. Segev, Y. Myasoedov, M. L. Rappaport, M. E. Huber, and E. Zeldov, A scanning superconducting quantum interference device with single electron spin sensitivity, *Nat. Nanotech.* **8**, 639 (2013).
  - [4] F. Giazotto, J. T. Peltonen, M. Meschke, and J. P. Pekola, Superconducting quantum interference proximity transistor, *Nat. Phys.* **6**, 254 (2010).
  - [5] M. Meschke, J. T. Peltonen, J. P. Pekola, and F. Giazotto, Tunnel spectroscopy of a proximity Josephson junction, *Phys. Rev. B* **84**, 214514 (2011).
  - [6] A. Ronzani, C. Altimiras, and F. Giazotto, Highly Sensitive Superconducting Quantum-Interference Proximity Transistor, *Phys. Rev. Appl.* **2**, 024005 (2014).

- [7] R. N. Jabdaraghi, M. Meschke, and J. P. Pekola, Non-hysteretic superconducting quantum interference proximity transistor with enhanced responsivity, *Appl. Phys. Lett.* **104**, 082601 (2014).
- [8] S. D'Ambrosio, M. Meissner, C. Blanc, A. Ronzani, and F. Giazotto, Normal metal tunnel junction-based superconducting quantum interference proximity transistor, *Appl. Phys. Lett.* **107**, 113110 (2015).
- [9] R. N. Jabdaraghi, J. T. Peltonen, O.-P. Saira, and J. P. Pekola, Low-temperature characterization of Nb-Cu-Nb weak links with Ar ion-cleaned interfaces, *Appl. Phys. Lett.* **108**, 042604 (2016).
- [10] R. N. Jabdaraghi, D. S. Golubev, J. P. Pekola, and J. T. Peltonen, Noise of a superconducting magnetic flux sensor based on a proximity Josephson junction, *Sci. Rep.* **7**, 8011 (2017).
- [11] P. Virtanen, A. Ronzani, and F. Giazotto, Spectral Characteristics of a Fully Superconducting SQUIPT, *Phys. Rev. Appl.* **6**, 054002 (2016).
- [12] A. Ronzani, S. D'Ambrosio, P. Virtanen, F. Giazotto, and C. Altimiras, Phase-driven collapse of the cooper condensate in a nanosized superconductor, *Phys. Rev. B* **96**, 214517 (2017).
- [13] N. Ligato, G. Marchegiani, P. Virtanen, E. Strambini, and F. Giazotto, High operating temperature in V-based superconducting quantum interference proximity transistors, *Sci. Rep.* **7**, 8810 (2016).
- [14] P. G. De Gennes, *Superconductivity of Metals and Alloys*, Advanced Book Classics (Perseus, Cambridge, MA, 1999).
- [15] A. I. Buzdin, Proximity effects in superconductor-ferrimagnet heterostructures, *Rev. Mod. Phys.* **77**, 935 (2005).
- [16] F. Zhou, P. Charlat, B. Spivak, and B. Pannetier, Density of states in superconductor-normal metal-superconductor junctions, *J. Low Temp. Phys.* **110**, 841 (1998).
- [17] F. Giazotto and F. Taddei, Hybrid superconducting quantum magnetometer, *Phys. Rev. B* **84**, 214502 (2011).
- [18] A. A. Golubov, M. Y. Kupriyanov, and E. Il'ichev, The current-phase relation in Josephson junctions, *Rev. Mod. Phys.* **76**, 411 (2004).
- [19] K. K. Likharev, Superconducting weak links, *Rev. Mod. Phys.* **51**, 101 (1979).
- [20] H. le Sueur, P. Joyez, H. Pothier, C. Urbina, and D. Esteve, Phase Controlled Superconducting Proximity Effect Probed by Tunneling Spectroscopy, *Phys. Rev. Lett.* **100**, 197002 (2008).
- [21] T. T. Heikkilä, J. Särkkä, and F. K. Wilhelm, Supercurrent-carrying density of states in diffusive mesoscopic Josephson weak links, *Phys. Rev. B* **66**, 184513 (2002).
- [22] N. Ligato, E. Strambini, F. Paolucci, and F. Giazotto, Preliminary demonstration of a persistent Josephson phase-slip memory cell with topological protection, *Nat. Commun.* **12**, 5200 (2021).
- [23] M. Polini, F. Giazotto, K. C. Fong, I. M. Pop, C. Schuck, T. Boccali, G. Signorelli, M. D'Elia, R. H. Hadfield, and V. Giovannetti, *et al.*, Materials and devices for fundamental quantum science and quantum technologies, (2022), arXiv preprint [ArXiv:2201.09260](https://arxiv.org/abs/2201.09260).
- [24] I. O. Kulik and A. N. Omel'yanchuk, Contribution to the microscopic theory of the Josephson effect in superconducting bridges, *JEPT Lett.* **21**, 96 (1975).
- [25] V. K. Kornev, I. I. Soloviev, N. V. Klenov, and O. A. Mukhanov, Bi-SQUID: a novel linearization method for dc SQUID voltage response, *Supercond. Sci. Technol.* **22**, 114011 (2009).
- [26] G. De Simoni, L. Cassola, N. Ligato, G. C. Tettamanzi, and F. Giazotto, Ultrahigh Linearity of the Magnetic-Flux-to-Voltage Response of Proximity-Based Mesoscopic Bi-SQUIDs, *Phys. Rev. Appl.* **18**, 014073 (2022).
- [27] S. N. Artemenko, A. F. Volkov, and A. V. Zaitsev, Theory of nonstationary Josephson effect in short superconducting contacts, *Sov. Phys. JEPT* **49**, 924 (1979).
- [28] R. C. Dynes, J. P. Garno, G. B. Hertel, and T. P. Orlando, Tunneling Study of Superconductivity Near the Metal-Insulator Transition, *Phys. Rev. Lett.* **53**, 2437 (1984).
- [29] M. Tinkham, *Introduction to Superconductivity* (Courier Dover Publications, New York, 2012).
- [30] J. R. Kirtley, Fundamental studies of superconductors using scanning magnetic imaging, *Rep. Prog. Phys.* **73**, 126501 (2010).
- [31] V. Ambegaokar and A. Baratoff, Tunneling between Superconductors, *Phys. Rev. Lett.* **10**, 486 (1963).
- [32] F. Giazotto, T. T. Heikkilä, G. P. Pepe, P. Helistö, A. Luukanen, and J. P. Pekola, Ultrasensitive proximity Josephson sensor with kinetic inductance readout, *Appl. Phys. Lett.* **92**, 162507 (2008).
- [33] A. Barone and G. Paterno, *Physics and Applications of Josephson Effect* (Wiley, New York, 1982).
- [34] C. Guarcello, P. Solinas, A. Braggio, M. Di Ventra, and F. Giazotto, Josephson Thermal Memory, *Phys. Rev. Appl.* **9**, 014021 (2018).
- [35] P. Solinas, M. Möttönen, J. Salmilehto, and J. P. Pekola, Cooper-pair current in the presence of flux noise, *Phys. Rev. B* **85**, 024527 (2012).